Eur. Phys. J. D **40**, 81–89 (2006)
DOI: 10.1140/epjd/e2006-00132-1

THE EUROPEAN PHYSICAL JOURNAL D

Hyperfine structure and isotope shifts in near-infrared transitions of atomic nitrogen

R.M. Jennerich[a], A.N. Keiser[b], and D.A. Tate[c]

Department of Physics and Astronomy, Colby College, Waterville, ME 04901, USA

Received 24 March 2006 / Received in final form 2nd May 2006
Published online 15 June 2006 –

Abstract. We have obtained Doppler-free spectra of transitions in the $2p^2(^3\mathrm{P})\ 3s\ ^4\mathrm{P} \rightarrow 2p^2(^3\mathrm{P})\ 3p\ ^4\mathrm{P}^\circ$ and $2p^2(^3\mathrm{P})\ 3s\ ^4\mathrm{P} \rightarrow 2p^2(^3\mathrm{P})\ 3p\ ^4\mathrm{D}^\circ$ multiplets of atomic nitrogen using saturated absorption spectroscopy. These multiplets consist of respectively of seven and eight transitions, and have center of gravity wavelengths of 821 nm and 869 nm. Values for the hyperfine structure coupling constants of all the upper and lower states for these multiplets were obtained for both ^{14}N and ^{15}N. Isotope shifts of three transitions in each multiplet were also measured, and a significant J-dependence to the shifts was observed.

PACS. 32.10.Fn Fine and hyperfine structure – 32.30.Jc Visible and ultraviolet spectra

1 Introduction

While a number of studies of lifetime dynamics in excited configurations of atomic nitrogen have been published in recent years [1–5], spectroscopic measurements that yield information on hyperfine structure (HFS) have largely been confined to states of the ground configuration using microwave and radio-frequency (rf) techniques [6–10]. In particular, there has been extensive interest in the $2p^3\ ^4\mathrm{S}_{3/2}$ ground state: if the three $2p$ electrons are purely LS coupled, both the magnetic dipole and electric quadrupole HFS coupling constants, A and B respectively, are expected to be zero. However, precise measurements on the $2p^3\ ^4\mathrm{S}_{3/2}$ state of ^{14}N have shown that $A = 10.45$ MHz and $B = 1.27$ Hz [8]. This is due to polarization of the closed $1s$ and $2s$ orbitals by the three $2p$ electrons which mixes the $2p$ sub-shell with other orbitals. Several theoretical papers have addressed this issue [11,12].

Most of the measurements of HFS and isotope shifts (IS) made in excited configurations of N are old, and were made using conventional Doppler-limited spectroscopic techniques [13–15]. The high temperatures associated with production processes for atomic N result in Doppler widths that make resolution of HFS and IS difficult in optical transitions. Several years ago, however, Cangiano et al. [16] measured HFS constants and isotope shifts for transitions of the $2p^2(^3\mathrm{P})\ 3s\ ^4\mathrm{P}_J \rightarrow 2p^2(^3\mathrm{P})\ 3p\ ^4\mathrm{P}^\circ_{J'}$ multiplet of ^{14}N and ^{15}N near 821 nm using an external cavity diode laser and Doppler-free techniques. (Throughout this paper, we use primed quantities J' and F' to represent angular momenta of the higher energy state of a particular transition, and unprimed quantities J and F to describe the lower energy state. In addition, all wavelengths are vacuum values.) To our knowledge, these were the first measurements made in excited states of nitrogen using Doppler-free techniques. While resolved hyperfine structure was visible in several of the components of this multiplet (shown schematically in Fig. 1), Cangiano found that the resolution of the spectra was limited to ≈200 MHz by the ≈70 MHz natural linewidth of the transitions and by collision broadening due to the relatively high pressures (∼1 torr) needed to maintain efficient nitrogen atom production and excitation in their rf discharge. While these factors allowed HFS coupling constants for ^{14}N and ^{15}N to be found for only the $^4\mathrm{P}_{3/2}$ (^{15}N only), $^4\mathrm{P}_{5/2}$, $^4\mathrm{P}^\circ_{1/2}$ (^{15}N only), $^4\mathrm{P}^\circ_{3/2}$, and $^4\mathrm{P}^\circ_{5/2}$ states, IS measurements were made for six of the seven transitions in this multiplet. The IS measurements suggested a relatively strong variation of the Specific Mass Shift (SMS = measured IS – normal mass shift) from one multiplet component to the next. For instance, the $^4\mathrm{P}_{5/2} \rightarrow {}^4\mathrm{P}^\circ_{3/2}$ IS was measured to be -1901 ± 150 MHz, but the $^4\mathrm{P}_{3/2} \rightarrow {}^4\mathrm{P}^\circ_{5/2}$ shift was found to be -1235 ± 150 MHz.

The findings of Cangiano et al. raise several intriguing issues. The main issue is whether the unusual variation of the IS between fine structure transitions in the

[a] *Present address:* BioArray Solutions Ltd., 35 Technology Drive, Suite 100, Warren, NJ 07059, USA.
[b] *Present address:* Science Department, New Hampton School, New Hampton, NH 03256, USA.
[c] e-mail: datate@colby.edu

$^4P_J \rightarrow {}^4P^\circ_{J'}$ multiplet is manifested in other multiplets in nitrogen. A second consideration is why the spectral resolution was not closer to the expected natural linewidths. Solution of these issues is principally related to improving the spectral resolution and obtaining spectra of other multiplets, and these considerations were the main motivation for the work described in this paper. In the course of our research, we found some interesting spectral perturbations in the Doppler-free spectra that we attribute to complex population dynamics in our discharge, and also to natural lifetime effects. We also identified some errors of presentation in the published results of Cangiano et al. An example of this is that the measured HFS splittings of the various F levels of the $^4P_{5/2}$ and $^4P^\circ_{3/2}$ states in Table I of reference [16] do not correctly reproduce the magnetic dipole and electric quadrupole coupling constants of these states as they are tabulated in Table II of that paper. There are also minor errors of presentation in some of the spectra. Specifically, the assigned F values in the schematic showing the HF energy levels for the $^4P^\circ_{5/2}$ state of the $^4P_{5/2} \rightarrow {}^4P^\circ_{5/2}$ transition in Figure 6a are incorrect, as are also the F values for the $^4P_{3/2}$ state of the $^4P_{3/2} \rightarrow {}^4P^\circ_{1/2}$ transition in Figure 6b. Furthermore, in the case of Figure 6a, the number of allowed HF transitions is wrong (six, when there should be seven), and their relative intensities are those appropriate for the $^4P_{5/2} \rightarrow {}^4P^\circ_{3/2}$ transition, not the $^4P_{5/2} \rightarrow {}^4P^\circ_{5/2}$ transition whose spectrum is shown in this figure.

The present paper describes our own study of the $2p^2$ (^{3}P) $3s$ ^{4}P $\rightarrow$ $2p^2(^3\mathrm{P})$ $3p$ ^{4}P° multiplet of atomic nitrogen, and an associated study of the $2p^2(^3\mathrm{P})$ $3s$ ^{4}P $\rightarrow$ $2p^2(^3\mathrm{P})$ $3p$ ^{4}D° multiplet, using Doppler-free saturated absorption spectroscopy. The paper is organized as follows. We describe first the apparatus and data acquisition procedure. We then discuss our analysis of the spectra of the two multiplets, and give values for HF coupling constants and isotope shifts obtained from the spectra. Finally, we consider experimental issues that became apparent during the course of this work that affected our ability to extract more data from the spectra, and which are the subject of ongoing research.

2 Experiment

The experimental apparatus used in this work is essentially the same as that used in previous studies of atomic fluorine, chlorine and oxygen [17–19]. A homemade external-cavity diode laser produced a few milliwatts of light [20]. Two different diodes were used in the external cavity: a Sharp LTO15 laser for the 821 nm spectra and a Spectra Diode Labs SDL-5401 laser at 869 nm. Each laser had a spectral linewidth of order 1 MHz when used in the external cavity, and was tunable over a range of ∼3 GHz. The Doppler-free absorption signal due to the nitrogen atoms was observed using standard saturated absorption techniques. The pump and probe laser beams passed longitudinally through the 6-inch-long discharge region, crossing near the center. The pump and probe laser beams were focussed using a 1-meter focal length lens, leading to a maximum intensity for the pump beam of ∼10 mW/mm^2, and ∼1 mW/mm^2 for the probe beam. The frequency scale of the laser scan was calibrated using a temperature stabilized confocal etalon with a free spectral range of 150.127 MHz. Nitrogen atoms were generated in excited states from molecular nitrogen in a low pressure (less than 1 torr) microwave discharge [21]. The discharge was sustained in a dilute gas mix that contained a maximum of 10–20% nitrogen, the rest being helium or argon. Simultaneous spectra of both stable isotopes were obtained by introducing both $^{14}N_2$ from a standard lecture bottle and $^{15}N_2$ from a 99.6 atomic-% isotopically enriched sample. The spectra were acquired using a digitizing oscilloscope and transferred to a computer. The raw data were then analyzed using a commercial software package. Reference [19] details our technique for obtaining the relevant frequency measurements and uncertainties. The one difference from our previous apparatus is that light from the laser was conveyed to the saturated absorption spectrometer by single mode optical fiber. The polarization of the light was restored at the output end using a quarter-wave plate and a linear polarizer. The transmission factor was usually around 30%, and the power at the output end was between 2–5 mW depending on the diode and the operation wavelength.

A schematic partial energy level diagram of nitrogen showing the quartet states of the $2p^2$ (^{3}P) $3s$ and $2p^2$ (^{3}P) $3p$ configurations is given in Figure 1. (For reference, the energies of the centers of gravity of these states, relative to the $2p^3$ $^4S_{3/2}$ ground state are: ^{4}P, 83 335.60 cm^{-1}; ^{4}S°, 96 750.84 cm^{-1}; ^{4}P°, 95 509.86 cm^{-1}; and ^{4}D°, 94 837.78 cm^{-1} [23].) The lower $2p^2$ $3s$ ^4P_J states have strong UV transitions to the $2p^3$ $^4S^\circ_{3/2}$ ground state at wavelengths around 120 nm. The lifetime of the $3s$ ^{4}P state has been measured by several research groups. The most recent experimental value, to our knowledge, is that of Goldbach et al. [4], who obtained 2.390 ns. The two most recent values of a $3p$ ^{4}D° state lifetime are those of Bengtsson et al. [1] and Copeland et al. [3], who give 44 ± 2 ns and 43 ± 3 ns respectively for the $^4D^\circ_{7/2}$ state. Finally, the most recent measurement for a $3p$ ^{4}P° state lifetime is 33 ns for the $^4P^\circ_{5/2}$ state [2], though a value of 55±5 ns was previously measured by Bromander et al. [5]. Combining these numbers, we expect natural linewidths of the Doppler-free spectra of approximately 70 MHz for both the $3s$ $^4P_J \rightarrow 3p$ $^4D^\circ_{J'}$ and $3s$ $^4P_J \rightarrow 3p$ $^4P^\circ_{J'}$ transitions.

Examples of our Doppler-free spectra for members of this multiplet are shown in Figure 2. The spectra shown are all the result of a single data scan with the exception of the $^4P_{5/2} \rightarrow {}^4D^\circ_{3/2}$ transition (Fig. 2e), for which the spectra shown are averages of 24 and 30 data scans respectively for the ^{15}N and ^{14}N isotopes. The reason for this is that the transition is so weak that individual spectra were very noisy. In addition, for this transition, laser scanning difficulties meant that we had to obtain spectra

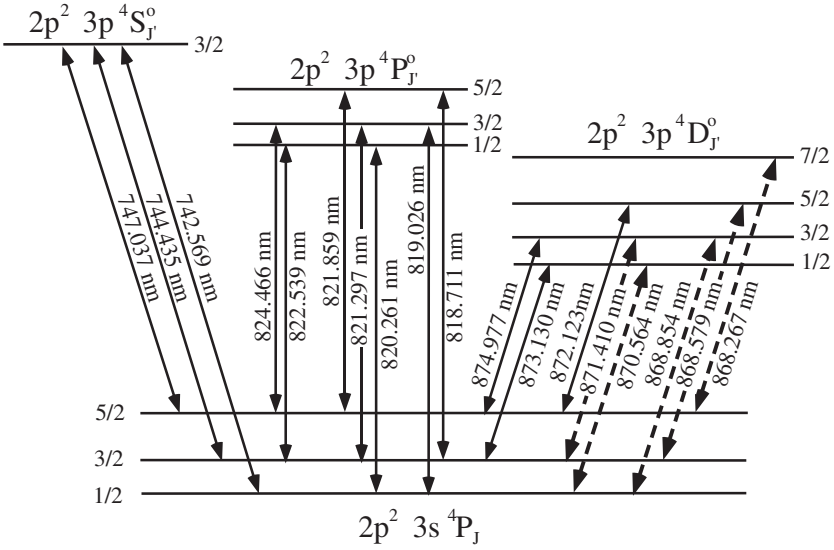

Fig. 1. Schematic partial energy level diagram of the $2p^2\ 3s\ ^4\mathrm{P}$, $2p^2\ 3p\ ^4\mathrm{S}^\circ$, $2p^2\ 3p\ ^4\mathrm{P}^\circ$, and $2p^2\ 3p\ ^4\mathrm{D}^\circ$ states showing allowed electric dipole transitions that connect these states. Transitions denoted by dashed lines in the $3s\ ^4\mathrm{P} \rightarrow 3p\ ^4\mathrm{D}^\circ$ multiplet have been identified as laser transitions [22]. The energies of the centers of gravity of these states, relative to the $2p^3\ ^4\mathrm{S}_{3/2}$ ground state are: $^4\mathrm{P}$, 83 335.60 cm^{-1}; $^4\mathrm{S}^\circ$, 96 750.84 cm^{-1}; $^4\mathrm{P}^\circ$, 95 509.86 cm^{-1}; and $^4\mathrm{D}^\circ$, 94 837.78 cm^{-1} [23].

of the two isotopes separately, and consequently we were unable to measure the isotope shift of this transition (the ^{14}N and ^{15}N spectra in Figure 2e are shown separated by an arbitrary IS of –1700 MHz).

3 Analysis

The spectra in Figure 2 were fitted to extract a complete set of A and B values for the ^{4}P, ^{4}P°, and ^{4}D° states, and IS values for six transitions, and we discuss these data first. In each spectrum in Figure 2, the distinct group of transitions at lower frequency is due to ^{15}N, while the group at higher frequency is due to ^{14}N (i.e., the isotope shift is negative). In Figure 2, the dots represent the data points, and the line is the fit that comprises a sum of Voigt profiles with amplitudes and positions that are floated in the fit. The residuals (data minus fit) are shown on a separate axis above each spectrum. The various HF components are identified by letter in each isotope, and these letters correspond to the individual HF transitions shown in the appropriate energy level diagrams that correspond to these transitions shown in Figure 3 (^{14}N) and Figure 4 (^{15}N). The spectra were fitted to obtain A and B values for the upper and lower states directly, and also to find the center of gravity of the ^{14}N and ^{15}N spectra. Initial guesses for these parameters were obtained by identifying the F values of the upper and lower state of several HF components based on their relative intensities, as described below. The A and B constants that are obtained from this analysis are shown in Table 1, and the isotope shifts in Table 2.

The Lorentzian widths are fixed to be equal for each isotope's transitions, and the resulting fit showed a negligible difference (≈2 MHz) for the ^{14}N and ^{15}N widths. The Gaussian partial widths were fixed at 6 MHz full width at half maximum (FWHM), as estimated from the laser beam crossing angle and the Doppler-limited absorption widths. (However, the quality of fit and Lorentzian partial widths were highly insensitive to the value used for the Gaussian partial width.) The minimum FWHM Lorentzian widths we found were approximately 75 MHz, though we more commonly observed Lorentzian widths of 80–90 MHz, which is consistent with the expected natural widths discussed above. Cangiano et al. [16] found a pressure-dependent broadening of 123 ± 5 MHz/Torr, and the minimum widths of their published spectra is approximately 200 MHz at a pressure of 1 Torr. The minimum pressure at which we were able to observe spectra was around 0.15 Torr, so our observed widths are consistent with the theoretical natural linewidths and a pressure broadening that is somewhat less than that observed by Cangiano et al. All of our spectra were obtained at total gas pressures between 0.15 and 1.0 Torr, and in this range, we observed no pressure dependent changes of the isotope shift or the A and B values obtained from the spectra. We interpret this finding as meaning that the hyperfine transition pressure shifts were equal within a given multiplet, and equal for both isotopes, or negligible. Unfortunately, the long-term temperature stability of our calibration etalon was not sufficient to measure the absolute pressure shift of a transition multiplet.

The spectra shown in Figure 2 provide a minimum data set from which we were able to extract the A and B values for all the ^{4}P, ^{4}P°, and ^{4}D° states. However, two factors complicated analysis of the spectra. First, at least one, and often more, of the HF components in each transition are poorly resolved due to the comparable sizes of the HF splittings and the transition natural linewidths. Second, for the combinations of J, J' and I values in these multiplets, two or three HF components are usually relatively strong (40% or more relative to the strongest HF component), while anywhere from one to four of the components (depending on the isotope and multiplet in question) have weak and comparable intensities (19% or less of the strongest HF component). This fact means that, while

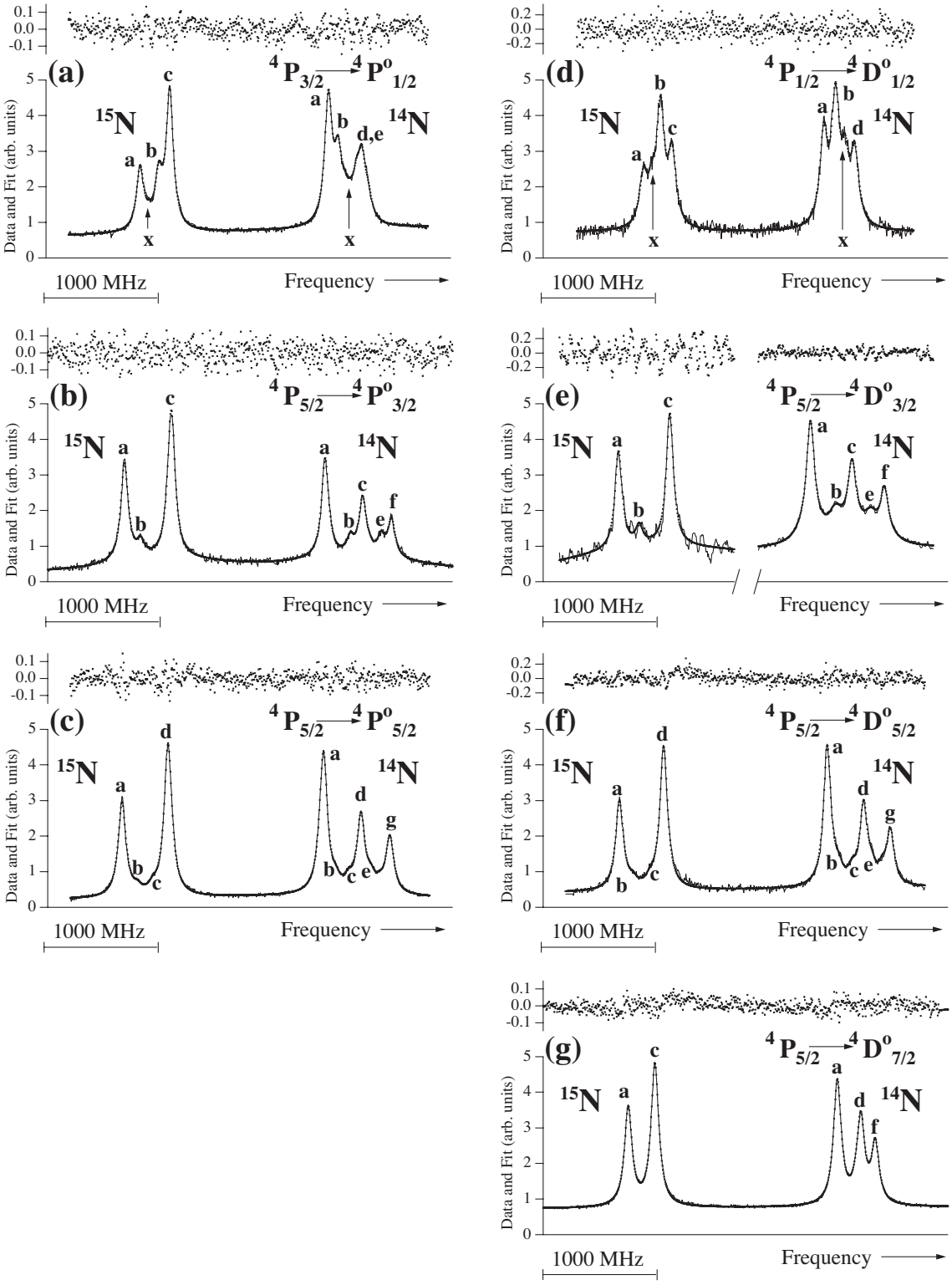

Fig. 2. Fitted Doppler-free spectra of several of the $^4P_J \rightarrow {}^4P^\circ_{J'}$ and $^4P_J \rightarrow {}^4D^\circ_{J'}$ multiplets in atomic nitrogen: $^4P_{3/2} \rightarrow {}^4P^\circ_{1/2}$ at $\lambda_{\rm vacuum} = 822.539$ nm (a); $^4P_{5/2} \rightarrow {}^4P^\circ_{3/2}$ at 824.466 nm (b); $^4P_{5/2} \rightarrow {}^4P^\circ_{5/2}$ at 821.859 nm (c); $^4P_{1/2} \rightarrow {}^4D^\circ_{1/2}$ at 870.564 nm (d); $^4P_{5/2} \rightarrow {}^4D^\circ_{3/2}$ at 874.977 nm (e); $^4P_{5/2} \rightarrow {}^4D^\circ_{5/2}$ at 872.123 nm (f); and $^4P_{5/2} \rightarrow {}^4D^\circ_{7/2}$ at 868.267 nm (g). The dots are the data, the line is the result of the fit, and residuals (data minus fit) are shown above the spectra. The arbitrary units of the data and residuals correspond within each spectrum, but the scale of the residuals is expanded differently for different spectra. The individual HF $F \rightarrow F'$ components are identified by letter according to the scheme shown in Figures 3 (for ^{14}N) and 4 (for ^{15}N). Crossover resonances are denoted by the $\times$ symbol.

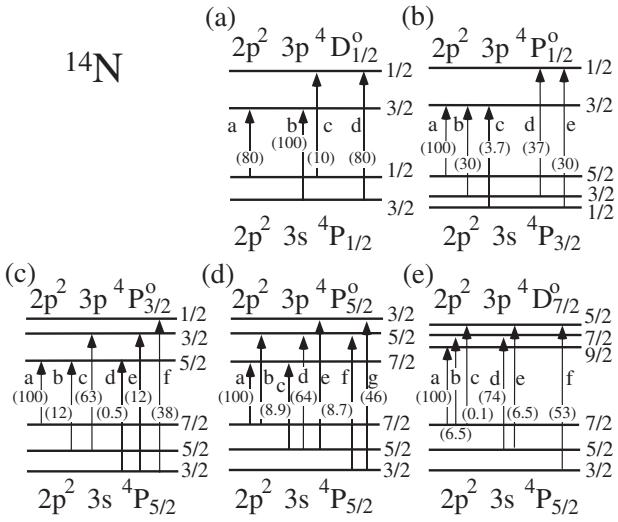

Fig. 3. Schematic diagrams of the HFS of the upper and lower levels of ^{14}N in the ^{4}P $\rightarrow$ ^{4}P° and ^{4}P $\rightarrow$ ^{4}D° transitions shown in Figure 2. (Note that the HFS diagrams for the $2p^2\ 3s\ ^4P_{5/2} \rightarrow 2p^2\ 3p\ ^4D^\circ_{3/2}$ and $2p^2\ 3s\ ^4P_{5/2} \rightarrow 2p^2\ 3p\ ^4D^\circ_{5/2}$ transitions shown in Figs. 2e and 2f are the same as those for the $2p^2\ 3s\ ^4P_{5/2} \rightarrow 2p^2\ 3p\ ^4P^\circ_{3/2}$ and $2p^2\ 3s\ ^4P_{5/2} \rightarrow 2p^2\ 3p\ ^4P^\circ_{5/2}$ transitions respectively.) Letters (a, b, c, etc.) represent the F values connected by a particular HF component for ^{14}N: for instance, in (b), b represents the $F = 3/2 \rightarrow F' = 3/2$ component of the $^4P_{3/2} \rightarrow {}^4P_{1/2}$ transitions, which appears in the Doppler-free ^{14}N (right hand side) $^4P_{3/2} \rightarrow {}^4P^\circ_{1/2}$ spectrum of Figure 2a as the peak identified by the letter b. The numbers in brackets on the individual transitions are their calculated relative intensities within the multiplet. (In (d) features b and c have the same strength, as do features e and f.)

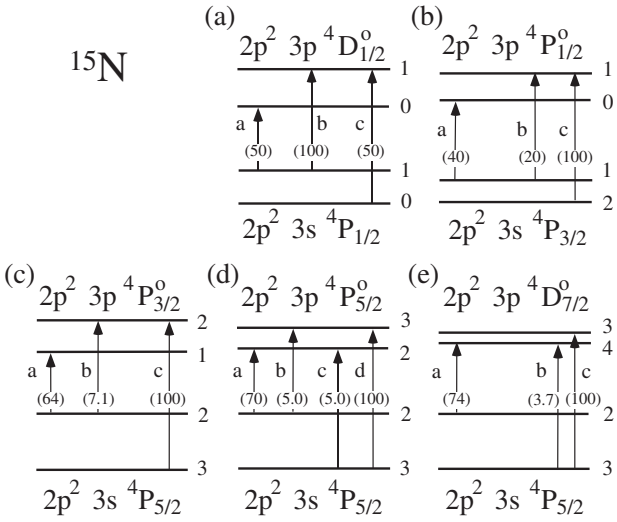

Fig. 4. Schematic diagrams of the HFS of the upper and lower levels of ^{15}N in the ^{4}P $\rightarrow$ ^{4}P° and ^{4}P $\rightarrow$ ^{4}D° transitions shown in Figure 2. (Note that the HFS diagrams for the $2p^2\ 3s\ ^4P_{5/2} \rightarrow 2p^2\ 3p\ ^4D^\circ_{3/2}$ and $2p^2\ 3s\ ^4P_{5/2} \rightarrow 2p^2\ 3p\ ^4D^\circ_{5/2}$ transitions shown in Figs. 2e and 2f are the same as those for the $2p^2\ 3s\ ^4P_{5/2} \rightarrow 2p^2\ 3p\ ^4P^\circ_{3/2}$ and $2p^2\ 3s\ ^4P_{5/2} \rightarrow 2p^2\ 3p\ ^4P^\circ_{5/2}$ transitions respectively.) Letters (a, b, c, etc.) represent the F values connected by a particular HF component for ^{15}N: for instance, in (b), b represents the $F = 1 \rightarrow F' = 1$ component of the $^4P_{3/2} \rightarrow {}^4P_{1/2}$ transitions, which appears in the Doppler-free ^{15}N (left hand side) $^4P_{3/2} \rightarrow {}^4P^\circ_{1/2}$ spectrum of Figure 2a as the peak identified by the letter b. The numbers in brackets on the individual transitions are their calculated relative intensities within the multiplet.

the strong HF lines are relatively easy to identify according to their F and F' values, the weak components are harder to identify unambiguously. This matter is in theory further complicated by the possible existence of crossover resonances as a consequence of the saturated absorption technique; however, we found such features in only two transitions during the course of this work.

One advantage in interpreting these spectra is that the ^{14}N and ^{15}N nuclear magnetic dipole moments are well known. Since the A values of a given state for the two isotopes should be in the ratio of the nuclear magnetic dipole moments, giving $A(15)/A(14) = -1.4028$ [7], one can test the consistency of the spectral line identifications. Using this fact, and the relative simplicity of the $^4P_{3/2} \rightarrow {}^4P^\circ_{1/2}$ (Fig. 2a) and $^4P_{5/2} \rightarrow {}^4P^\circ_{3/2}$ (Fig. 2b) spectra, we were able to unambiguously identify F and F' values for the individual HF components in these spectra, allowing us to extract initial A and B values for these states. In addition, the fits of the $^4P_{5/2} \rightarrow {}^4D^\circ_{5/2}$ spectrum (Fig. 2f) independently confirmed the A and B values of the $^4P_{5/2}$ state (for both isotopes), and this information was then used to find A and B values for the upper states in the $^4P_{5/2} \rightarrow {}^4P^\circ_{5/2}$ (Fig. 2c), $^4P_{5/2} \rightarrow {}^4D^\circ_{3/2}$ (Fig. 2e), and $^4P_{5/2} \rightarrow {}^4D^\circ_{7/2}$ (Fig. 2g) transitions. However, attribution of F and F' values for components of the $^4P_{1/2} \rightarrow {}^4D^\circ_{1/2}$ (Fig. 2d) transition is more difficult. The reason for this can be seen by considering the relative intensities of the HF components, which are 100:80:80:10 for ^{14}N and 100:50:50 in ^{15}N, as seen in Figure 3a for ^{14}N and Figure 4a for ^{15}N. In each isotope, two transitions have the same amplitude, preventing unambiguous attribution of the $F = 3/2 \rightarrow F' = 1/2$ and $F = 1/2 \rightarrow F' = 3/2$ components in ^{14}N, and the $F = 1 \rightarrow F' = 0$ and $F = 0 \rightarrow F' = 1$ components in ^{15}N. In principle, identification of the $F = 1/2 \rightarrow F' = 1/2$ component in the ^{14}N Doppler-free spectrum should be enough to resolve this issue. However, this component is only 10% of the strongest $F = 3/2 \rightarrow F' = 3/2$ component, and the signal-to-noise and natural lifetime limited resolution were insufficient to identify it. However, the presence of one crossover in each isotope (labelled "×" in Fig. 2d) provides a resolution to this problem. From our previous work on oxygen and chlorine [18,19], we find that such crossovers are more likely to share the same lower state, rather than to share a common upper state, and we used this fact to make the F and F' identification. As a result, we find that, for ^{14}N, $A(^4P_{1/2}) = -69.8$ MHz, and $A(^4D^\circ_{1/2}) = -112.3$ MHz, while for ^{15}N, $A(^4P_{1/2}) = +103.4$ MHz, and $A(^4D^\circ_{1/2}) = +153.1$ MHz, as shown in Table 1. (In the less probable situation, the F and F' attributions of the

Table 1. Magnetic dipole HFS constants (A) and electric quadrupole HFS constants (B) for the $3s\ ^4\mathrm{P}$, $3p\ ^4\mathrm{P}^\circ$, and $3p\ ^4\mathrm{D}^\circ$ levels of ^{14}N and ^{15}N. The errors quoted for our experimental data are one standard deviation of the mean.

	^{14}N		^{14}N		^{15}N	^{15}N
	This experiment		Previous work		This experiment	Previous work
Level	A (MHz)	B (MHz)	A (MHz)	B (MHz)	A (MHz)	A (MHz)
$3s\ ^4\mathrm{P}_{1/2}$	–69.76(90)	0.0			+103.4(14)	
	+112.3(13)[a]	0.0			–153.1(23)[a]	
$3s\ ^4\mathrm{P}_{3/2}$	+35.52(44)	–0.98(48)			–47.93(48)	+45(9)[b]
$3s\ ^4\mathrm{P}_{5/2}$	+64.76(42)	–3.9(10)	+61(5)[b]	–50(3)[b]	–90.71(71)	–82(5)[b]
			+65(3)[c]	0(7)[c]		
$3p\ ^4\mathrm{P}^\circ_{1/2}$	–133.2(22)	0.0			+167.1(13)	+154(10)[b]
$3p\ ^4\mathrm{P}^\circ_{3/2}$	–48.56(74)	+8.69(87)	–54(4)[b]	–23(3)[b]	+70.0(12)	+83(5)[b]
			–54(4)[c]	+9(3)[c]		
$3p\ ^4\mathrm{P}^\circ_{5/2}$	–32.83(44)	+5.0(11)			+46.20(74)	+53(6)[b]
$3p\ ^4\mathrm{D}^\circ_{1/2}$	–112.3(13)	0.0			+153.1(23)	
	+69.76(90)[a]	0.0			–103.4(14)[a]	
$3p\ ^4\mathrm{D}^\circ_{3/2}$	–64.41(79)	+10.46(88)			+92.4(17)	
$3p\ ^4\mathrm{D}^\circ_{5/2}$	–28.19(62)	–0.2(15)			+41.5(14)	
$3p\ ^4\mathrm{D}^\circ_{7/2}$	+6.31(72)	–12.6(13)			–9.35(55)	

[a] Data in this row are less likely possible A values to those reported in row immediately above. See text for details. [b] Data from Table II of reference [16]. [c] Data in this row represent values from the row immediately above corrected using data from Table I of reference [16].

Table 2. Experimental values of the isotope shifts of fitted transitions in Figure 2 (except $^4\mathrm{P}_{5/2} \rightarrow {}^4\mathrm{D}^\circ_{3/2}$). "Measured IS" = $\nu(^{15}\mathrm{N}) - \nu(^{14}\mathrm{N})$, where $\nu(^{15}\mathrm{N})$ and $\nu(^{14}\mathrm{N})$ are frequencies of the centers of gravity of the hyperfine multiplets for ^{15}N and ^{14}N respectively. Also given are calculated values for the normal mass shift (NMS). The errors quoted for our experimental data are one standard deviation of the mean. (We include results from other researchers for transitions that we did not measure ourselves for completeness, and also since we discuss some of these previous results in this paper.)

Transition	Measured IS (MHz) (This work)	Measured IS (MHz) (Previous work)	Measured IS (MHz) (Previous work)	NMS (MHz)
$^4\mathrm{P}_{1/2} \rightarrow {}^4\mathrm{P}^\circ_{3/2}$		–1518(150)[a]		+953.1
$^4\mathrm{P}_{3/2} \rightarrow {}^4\mathrm{P}^\circ_{1/2}$	–1609.3(22)	–1610(150)[a]	–1800(180)[b]	+949.0
$^4\mathrm{P}_{3/2} \rightarrow {}^4\mathrm{P}^\circ_{3/2}$		–1557(150)[a]		+950.5
$^4\mathrm{P}_{3/2} \rightarrow {}^4\mathrm{P}^\circ_{5/2}$		–1235(150)[a]		+953.5
$^4\mathrm{P}_{5/2} \rightarrow {}^4\mathrm{P}^\circ_{3/2}$	–1766.6(14)	–1901(150)[a]	–1788(18)[b]	+946.8
$^4\mathrm{P}_{5/2} \rightarrow {}^4\mathrm{P}^\circ_{5/2}$	–1795.6(18)	–1788(150)[a]	–1737(15)[b]	+949.8
$^4\mathrm{P}_{1/2} \rightarrow {}^4\mathrm{D}^\circ_{1/2}$	–1591.4(15)	–1800(300)[c]		+896.7
$^4\mathrm{P}_{5/2} \rightarrow {}^4\mathrm{D}^\circ_{5/2}$	–1853.07(84)	–1800(300)[c]		+895.1
$^4\mathrm{P}_{5/2} \rightarrow {}^4\mathrm{D}^\circ_{7/2}$	–1863.8(16)			+899.1

[a] Reference [16]. [b] Reference [14]. [c] Reference [15].

equal-intensity transitions in each isotope are switched. This results in different A values: for ^{14}N, $A(^4\mathrm{P}_{1/2}) = +112.3$ MHz, and $A(^4\mathrm{D}^\circ_{1/2}) = +69.8$ MHz, while for ^{15}N, $A(^4\mathrm{P}_{1/2}) = -153.1$ MHz, and $A(^4\mathrm{D}^\circ_{1/2}) = -103.4$ MHz. However, there is no change in the IS value we extract from the spectra. These less likely A values are given in Table 1 for completeness.) Unfortunately, the A and B values for the $^4\mathrm{P}_{1/2}$ and $^4\mathrm{D}^\circ_{1/2}$ states cannot be confirmed from our spectra of any other transition. We were unable to obtain a spectrum of the very weak $^4\mathrm{P}_{1/2} \rightarrow {}^4\mathrm{P}^\circ_{1/2}$ transition, and all the other transitions sharing either an upper or lower state with the $^4\mathrm{P}_{1/2} \rightarrow {}^4\mathrm{D}^\circ_{1/2}$ transition are subject to the kind of spectral perturbations shown in Figure 5 and discussed below in Section 4.2. Our spectra of the $^4\mathrm{P}_{1/2} \rightarrow {}^4\mathrm{P}^\circ_{3/2}$ (shown in Fig. 5a), $^4\mathrm{P}_{1/2} \rightarrow {}^4\mathrm{D}^\circ_{3/2}$, and $^4\mathrm{P}_{3/2} \rightarrow {}^4\mathrm{D}^\circ_{1/2}$ transitions were therefore unable to resolve the ambiguity of the values for A and B for the $^4\mathrm{P}_{1/2}$ and $^4\mathrm{D}^\circ_{1/2}$ states.

4 Discussion

First, we discuss the HF coupling constants shown in Table 1. Since the IS values are critically dependent on correct interpretation of the HFS of the ^{14}N and ^{15}N spectra, we leave the discussion of the IS values in Table 2 until the end of this paper. The experimental values given in Table 1

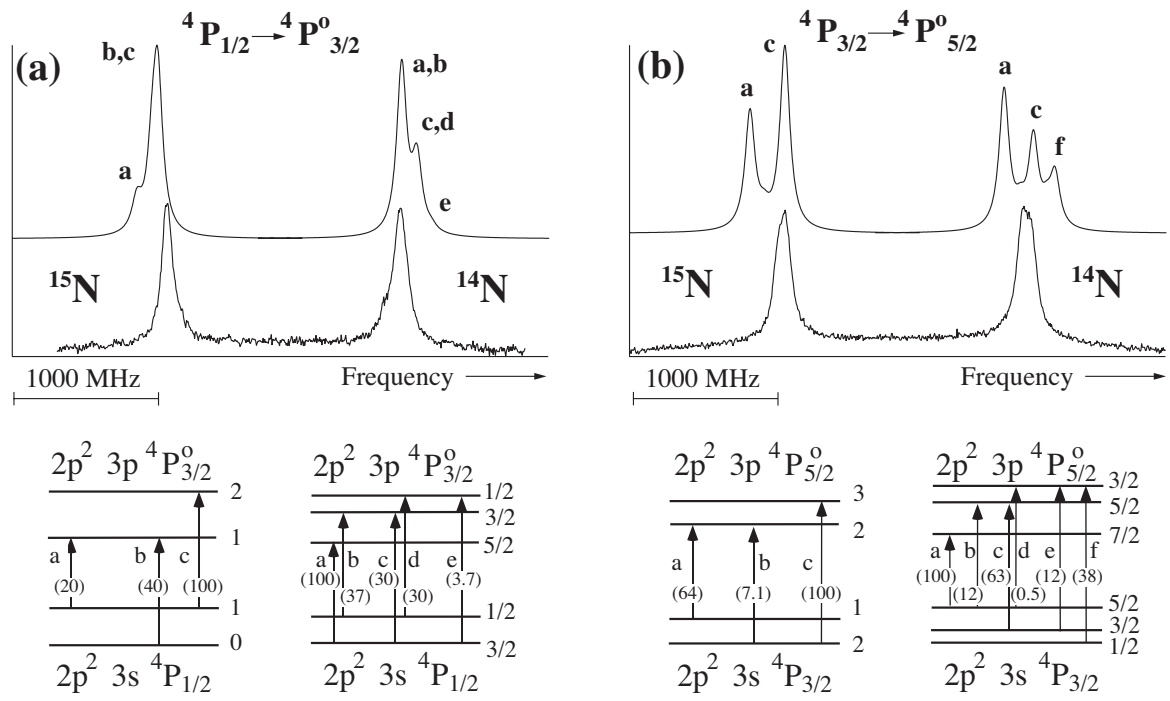

Fig. 5. Experimental and theoretical Doppler-free spectra of the $^4P_{1/2} \rightarrow {}^4P^\circ_{3/2}$ transition at $\lambda_{\rm vacuum} = 819.026$ nm (a); and the $^4P_{3/2} \rightarrow {}^4P^\circ_{5/2}$ transition at 818.711 nm (b), showing the intensity perturbations of the experimental spectra. In each spectrum, the lower trace is the experimental data, and the upper trace is the theoretical spectrum for the transition, based on the HFS coupling constants shown in Table 1, and arbitrarily setting the isotope shift to –1700 MHz. The individual HF $F \rightarrow F'$ components are identified by letter according to the scheme in the schematic HFS diagrams shown below each spectrum (at the bottom of each of (a) and (b), the diagram on the left is for ^{15}N and the diagram on the right is for ^{14}N). In each diagram of the HFS of the upper and lower levels, a letter identifies a particular HF transition, and the same letter identifies this transition in the synthesized spectrum of each isotope.

(and Tab. 2) are averages of the results of individual fits of spectra. (The uncertainties shown in round brackets, e.g., "(22)", in Tabs. 1 and 2 represent the random uncertainty, and are one standard deviation of the mean of the average values calculated from many data sets.) For each of the transitions shown in Figure 2, we obtained between 8 and 22 spectra that were fitted. The random uncertainty also incorporates the uncertainty inherent in our spectrum fitting programs and the frequency scale linearization uncertainty, as detailed in reference [18]. (The exception is the $^4P^\circ_{5/2} \rightarrow {}^4D^\circ_{3/2}$ spectrum, Figure 2e, which is an average of 24 spectra for ^{15}N and 30 spectra for ^{14}N: these average spectra were fitted just once. The uncertainty of parameters obtained from this fit therefore represents the fit and linearization uncertainties, since only one fit was performed for each isotope.)

4.1 HFS coupling constants

Our A and B values given in our Table 1 that are extracted from the spectra of three of the $^4P_J \rightarrow {}^4P^\circ_{J'}$ transitions (those shown in Figs. 2a–2c) generally agree with those of Cangiano et al. once their values reported in Table II of reference [16] are corrected to be consistent with the measured HFS intervals given in Table I of that paper. However, our values are more precise than Cangiano's, and we were also able to obtain values of the coupling constants of the $^4P_{3/2}$ and $^4P^\circ_{1/2}$ states for ^{14}N that Cangiano was unable to measure. In addition, we have data obtained from our spectra of the $^4P_J \rightarrow {}^4D^\circ_{J'}$ transitions that have not previously been studied using Doppler-free spectroscopy. The A values of a given state for the two isotopes are expected to have a ratio that is close to that of the magnetic dipole moments of their nuclei, $g(15)/g(14) = -1.4028$ [7]. When this ratio is calculated from our data in Table 1, we find that most of the values conform to this value within reasonable error limits based interpretation of the uncertainties in Table 1 as standard deviations. However, there are four states for which this is not true, namely the upper and lower states of the $^4P_{3/2} \rightarrow {}^4P^\circ_{1/2}$ and $^4P_{1/2} \rightarrow {}^4D^\circ_{1/2}$ transitions shown in Figures 2a and 2d respectively. Since our knowledge of these states is obtained from only these two transitions, and some of the HF components are only partially resolved, this is perhaps not so surprising. The ratios $A(15)/A(14)$ for $^4P_{1/2}$, $^4P_{3/2}$, and $^4D^\circ_{1/2}$ states lie between 1.5 and 3.0 standard deviations away from the mean of all the results, but that for $^4P^\circ_{1/2}$ is different from the mean by 6.7 standard deviations. If we omit this particular value, the weighted mean of the A-ratio for the other nine states is –1.404(9), in good agreement with

the expected value. We find that the relative intensities of the HF components that we obtain from our fit usually conform to those predicted (and shown in Figs. 3 and 4) within ±20%, with the occasional exception of very weak components (those with less than 10% of the intensity of strongest component) in partially resolved spectra.

4.2 Line shape perturbations

We have obtained spectra of other transitions in the $^4P_J \rightarrow {}^4P^\circ_{J'}$ and $^4P_J \rightarrow {}^4D^\circ_{J'}$ multiplets other than those shown in Figure 2. In general, however, these other transitions are subject to greater or lesser degrees of line shape perturbation. The main manifestation of this is that one or two of the HF components of a given transition become dominant, and the others become negligible in strength. Two examples of this are shown in Figure 5 which shows the $^4P_{1/2} \rightarrow {}^4P^\circ_{3/2}$ (Fig. 5a) and $^4P_{3/2} \rightarrow {}^4P^\circ_{5/2}$ (Fig. 5b). The Doppler-free spectra are shown, along with spectra synthesized from the data given in Table 1 (an arbitrary IS of –1700 MHz between the centers of gravity is assumed). As can be seen, the experimental spectra show only one or two unresolved components for each isotope, visible as asymmetries in the line shape. (In two other transitions, each isotope has two distinct but barely resolved peaks.) We show these spectra because they were previously observed by Cangiano et al. [16]. Spectra of the $^4P_{1/2} \rightarrow {}^4P^\circ_{3/2}$ transition that are essentially identical to ours are shown in Figure 6c (for ^{14}N) and Figure 7c (for ^{15}N) of Reference [16]. Like our data, no structure is discernable in Cangiano's spectra of this transition. Reference [16] gives an IS value for $^4P_{3/2} \rightarrow {}^4P^\circ_{5/2}$, as well as for $^4P_{3/2} \rightarrow {}^4P^\circ_{3/2}$, and these data are reported in Table III of that paper, but no spectra are shown for these two transitions.

We have ruled out the most obvious reasons for the differences between the observed and theoretical spectra. The most significant of these is the possibility that the data given in Table 1 are wrong as a result of improper assignment of HF components in the spectra shown in Figure 2. This possibility is ruled out by the fact that the fits shown in Figure 2 are so good, and the resulting transition strength ratios are very close to the theoretical values. Furthermore, different assignments of the F and F' values for a particular HF transition than those given in Figure 2 would lead to different A and B values, but these values would still predict that the transitions shown in Figure 5 would have clearly resolved structure, and they obviously do not. (The spectra shown in Figure 5 are typical for each transition. In other words, the perturbations seem to be independent of the gas pressure and microwave power.)

We believe that there are a number of possible contributing factors to the unusual line shapes shown in Figure 5. First, there are known laser transitions in atomic nitrogen on five of the $^4D^\circ_{J'} \rightarrow {}^4P_J$ transitions. Specifically, the $J' = 7/2 \rightarrow J = 5/2$, $J' = 5/2 \rightarrow J = 3/2$, $J' = 3/2 \rightarrow J = 1/2$, $J' = 3/2 \rightarrow J = 3/2$, and $J' = 1/2 \rightarrow J = 1/2$ transitions have been observed to exhibit laser action in a hollow cathode discharge either during the current pulse, or in the afterglow [22], in a laser medium of very dilute molecular nitrogen in helium at a total pressure of order 10 Torr. (These transitions are identified in Fig. 1.) It is therefore possible that lasing on one or more of these transitions leads to significant population depletion in some HF states and not others. (In our study of atomic fluorine, we observed some unusual line shape effects due to laser action [18].) Second, the energy separations of the different hyperfine sub-states of both the $^4P_{1/2}$ and $^4P_{3/2}$ state are comparable with the natural line widths of these states. The lifetime for the ^4P_J states of 2.390 ns reported in reference [4] translates to a width of 67 MHz, and the largest HF splittings of the $^4P_{1/2}$ and $^4P_{3/2}$ states are 100 MHz or less, based on the data in Table 1. Unusual line shape effects can occur in this limit, especially at higher pressures when the effects of collisional decoupling of the hyperfine states can occur [24]. In principle, the effects of laser transitions and natural lifetime effects may be modeled using density matrix techniques (see for instance the appendix of Ref. [25], and Ref. [26]). We are presently pursuing such theoretical studies of the saturated absorption line shapes of our perturbed spectra to more fully understand this phenomenon.

4.3 Isotope shifts

We now discuss the isotope shift values that we extracted from our spectra, which are given in Table 2, along with selected results of previous studies and values for the normal mass shifts (NMS) between the two isotopes for these transitions. The IS values given in Table 2 are derived from fits of the spectra shown in Figure 2 (except Fig. 2e).

Our isotope shift results given in Table 2 may be compared with those of Cangiano et al. [16], made using Doppler-free spectroscopy with an external cavity diode laser, and with those of Holmes made using a Fabry-Perot interferometer giving Doppler-limited resolution [14,15]. These comparisons are given in Table 2. Our results show good agreement with these previous works. Like Cangiano et al., we observe a significant variation of the isotope shift within each multiplet. However, we are unable to confirm the significantly different value of the $^4P_{3/2} \rightarrow {}^4P^\circ_{5/2}$ IS from those of the other transitions. Cangiano gives the value of this IS as -1235 ± 150 MHz. Since our spectra of this line are significantly perturbed as described above, we are unable to fit them to obtain an IS value. However, when we fit the spectrum of each isotope as a sum of two components with merged Voigt profiles, the center of the strongest ^{15}N component has a frequency of –1583(4) MHz relative to the strongest ^{14}N component, a value that is more than 300 MHz lower in magnitude than Cangiano's reported IS. (None of Cangiano's spectra shows a full scan over the ^{14}N and ^{15}N features, which are presented separately, and the method that was used to measure their IS values is not described. It is therefore not possible to discover how such a difference between our IS values can have arisen.)

We are also unable to present IS values for the $^4P_{1/2} \rightarrow {}^4P^\circ_{3/2}$ and $^4P_{3/2} \rightarrow {}^4P^\circ_{3/2}$ transitions, which

Cangiano gives as –1518(150) MHz and –1557(150) MHz respectively. Using the fitting protocol described in the previous paragraph, we find that the frequency of the strongest component in ^{15}N relative to the strongest component in ^{14}N is –1568(1) MHz for $^4\mathrm{P}_{1/2} \rightarrow {}^4\mathrm{P}^\circ_{3/2}$, and –1580(4) MHz for $^4\mathrm{P}_{3/2} \rightarrow {}^4\mathrm{P}^\circ_{3/2}$. These values are clearly in better agreement with Cangiano's numbers. However, a direct comparison is hard to make since there is significant perturbation in our spectra. Given the fact that Cangiano et al. show no spectra for these transitions, it is not possible to comment further on the extent of agreement or disagreement between our IS values and those of Cangiano et al. [16].

Nevertheless, our IS values show significant variations between transitions of the same multiplet. For instance, our Residual Isotope Shift (RIS = measured IS – NMS) values vary from –2558.3 MHz for $J = 3/2 \rightarrow J' = 1/2$ to –2745.8 MHz for $J = 5/2 \rightarrow J' = 5/2$ in the $^4\mathrm{P}_J \rightarrow {}^4\mathrm{P}^\circ_{J'}$ multiplet, and from –2488.1 MHz for $J = 1/2 \rightarrow J' = 1/2$ to –2762.9 MHz for $J = 5/2 \rightarrow J' = 7/2$ in the $^4\mathrm{P}_J \rightarrow {}^4\mathrm{D}^\circ_{J'}$ multiplet. The RIS is the sum of two components: the Specific Mass Shift (SMS) and the Field Shift (FS). Since the FS is significant only for heavy nuclei, the dominant term in the RIS in nitrogen is the SMS. As pointed out by Cangiano et al. [16], such a J-dependence of the RIS values has been attributed by Keller [27] to relativistic contributions and electron correlations affecting the SMS. In particular, Keller notes that Holmes' spectra of nitrogen [14] provide possible evidence for such effects making significant contributions to the RIS in nitrogen. Identification of such effects, which may only be calculated with precision for light atoms, has generally been limited by the availability of experimental data.

5 Conclusion

We have obtained Doppler-free spectra of transitions in the $2p^2(^3\mathrm{P})\,3s\,{}^4\mathrm{P} \rightarrow 2p^2(^3\mathrm{P})\,3p\,{}^4\mathrm{P}^\circ$ and $2p^2(^3\mathrm{P})\,3s\,{}^4\mathrm{P} \rightarrow 2p^2(^3\mathrm{P})\,3p\,{}^4\mathrm{D}^\circ$ multiplets of atomic nitrogen using saturated absorption spectroscopy with an external cavity diode laser. Using these spectra, we have measured IS between the two stable isotopes of atomic nitrogen in six of the transitions in the two multiplets. In addition, we have obtained experimental values for the magnetic dipole and electric quadrupole HF coupling constants of all of the ^{4}P, ^{4}P°, and ^{4}D° states of ^{14}N and ^{15}N. Our set of measurements is more extensive and generally more precise than previously published results, and we hope that these data will stimulate theoretical study of these states. Our isotope shift results reveal a significant J-dependence of the SMS in both multiplets, and we hope that these data will stimulate theoretical investigations of the underlying cause of this phenomenon. Finally, we find significant perturbation of some of the Doppler-free spectra that we attribute to laser transitions that occur in atomic nitrogen generated in the discharge environment, and also to natural lifetime effects. Modeling these line shapes is the subject of ongoing research.

Funding for these experiments has been provided by Colby College under the Division of Natural Sciences Faculty Research Grant program and by the NSF Academic Research Infrastructure program (grant number PHY-9601638). We acknowledge discussions with Per Jönsson, Jeff Dunham, and Mark Havey.

References

1. G.J. Bengtsson, J. Larsson, S. Svanberg, D.D. Wang, Phys. Rev. A **45**, 2712 (1992)
2. Q. Zhu, J.M. Bridges, T. Hahn, W.L. Wiese, Phys. Rev. A **40**, 3721 (1989)
3. R.A. Copeland, J.B. Jeffries, A.P. Hickman, D.R. Crosley, J. Chem. Phys. **86**, 4876 (1987)
4. C. Goldbach, M. Martin, G. Nollez, P. Plomdeur, J.P. Zimmermann, D. Babic, Astron. Astrophys. **161**, 47 (1986)
5. J. Bromander, N. Djurić, P. Erman, M. Larsson, Phys. Scr. **17**, 119 (1978)
6. M.A. Heald, R. Beringer, Phys. Rev. **96**, 645 (1954)
7. L.W. Anderson, F.M. Pipkin, J.C. Baird Jr, Phys. Rev. **116**, 87 (1959)
8. J.M. Hirsch, G.H. Zimmerman III, D.J. Larson, N.F. Ramsey, Phys. Rev. A **16**, 484 (1977)
9. G.J. Diebold, D.L. McFadden, Phys. Rev. A **25**, 1504 (1982)
10. V. Beltrán-López, J. Rangel, G.A. González-Nucamendi, J. Jiménez-Mier, A. Fuentes-Maya, Phys. Rev. A **39**, 58 (1989)
11. C.W. Bauschlicher, J. Chem. Phys. **92**, 518 (1990)
12. S.A. Perera, J.D. Watts, R.J. Bartlett, J. Chem. Phys. **100**, 1425 (1994)
13. R.F. Bacher, Phys. Rev. **43**, 1001 (1933)
14. J.R. Holmes, Phys. Rev. **63**, 41 (1943)
15. J.R. Holmes, J. Opt. Soc. Am. **41**, 360 (1951)
16. P. Cangiano, M. de Angelis, L. Gianfrani, G. Pesce, A. Sasso, Phys. Rev. A **50**, 1082 (1994)
17. D.A. Tate, D.N. Aturaliye, Phys. Rev. A **56**, 1844 (1997)
18. D.A. Tate, J.P. Walton, Phys. Rev. A **59**, 1170 (1999)
19. R.M. Jennerich, D.A. Tate, Phys. Rev. A **62**, 042506 (2000)
20. K.B. MacAdam, A. Steinbach, C. Wieman, Am. J. Phys. **60**, 1098 (1992)
21. F.C. Fehsenfeld, K.M. Evenson, H.P. Broida, Rev. Sci. Instrum. **36**, 294 (1965)
22. X. Zhu, J. Liu, F. Lin, Appl. Phys. B **29**, 111 (1982)
23. W.L. Wiese, J.R. Fuhr, T.M. Deters, *Atomic Transition Probabilities of Carbon, Nitrogen, and Oxygen: A Critical Data Compilation* (American Institute of Physics, Woodbury, NY, 1996)
24. E.W. Weber, Phys. Rev. A **20**, 2278 (1979)
25. P.R. Berman, D.G. Steel, G. Khitrova, J. Liu, Phys. Rev. A **38**, 252 (1988)
26. H.K. Holt, Phys. Rev. Lett. **29**, 1138 (1972)
27. J.C. Keller, J. Phys. B **6**, 1771 (1973)